JOURNAL OF Applied Polymer SCIENCE

Special Issue: Manufacturing of Advanced Biodegradable Polymeric Components

Guest Editors: Prof. Roberto Pantani (University of Salerno) and
Prof. Lih-Sheng Turng (University of Wisconsin–Madison)

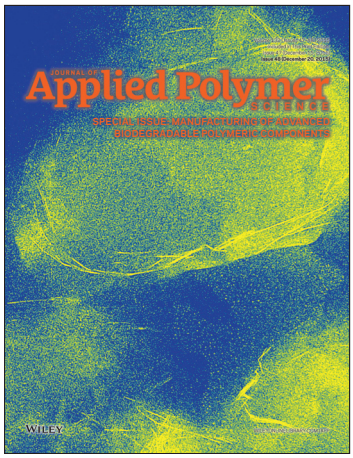

EDITORIAL

REVIEWS

ARTICLES

JOURNAL OF Applied Polymer SCIENCE

Special Issue: Manufacturing of Advanced Biodegradable Polymeric Components

Guest Editors: Prof. Roberto Pantani (University of Salerno) and Prof. Lih-Sheng Turng (University of Wisconsin–Madison)

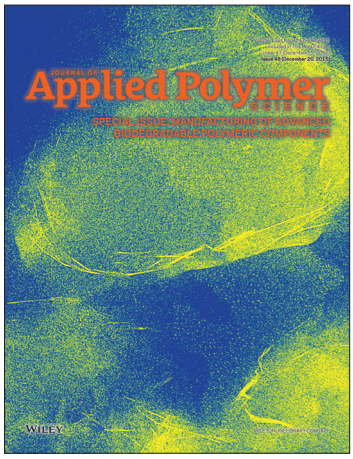

Rotational molding of biodegradable composites obtained with PLA reinforced by the wooden backbone of opuntia ficus indica cladodes
A. Greco and A. Maffezzoli, *J. Appl. Polym. Sci.* 2015, **DOI:** 10.1002/app.42447

Foam injection molding of poly(lactic) acid: Effect of back pressure on morphology and mechanical properties
V. Volpe and R. Pantani, *J. Appl. Polym. Sci.* 2015, **DOI:** 10.1002/app.42612

Modification and extrusion coating of polylactic acid films
H.-Y. Cheng, Y.-J. Yang, S.-C. Li, J.-Y. Hong and G.-W. Jang, *J. Appl. Polym. Sci.* 2015, **DOI:** 10.1002/app.42472

Processing and properties of biodegradable compounds based on aliphatic polyesters
M. R. Nobile, P. Cerruti, M. Malinconico and R. Pantani, *J. Appl. Polym. Sci.* 2015, **DOI:** 10.1002/app.42481

Journal of Applied Polymer Science

Reactive extrusion effects on rheological and mechanical properties of poly(lactic acid)/poly[(butylene succinate)-co-adipate]/epoxy chain extender blends and clay nanocomposites

Amin Mirzadeh,[1] Hesam Ghasemi,[2] Fatma Mahrous,[1] Musa R. Kamal[1]
[1]Department of Chemical Engineering, McGill University, Montreal, Quebec H3A 2B2, Canada
[2]Department of Chemistry and Chemical Engineering, Royal Military College, Kingston Ontario, Canada
Correspondence to: M. R. Kamal (E-mail: musa.kamal@mcgill.ca)

ABSTRACT: Poly(lactic acid) (PLA), a biosource, biodegradable polymer, is not suitable for some important polymer processing operations, such as film blowing and blow molding, due to its low melt strength. Moreover, while it has high tensile modulus and strength in the solid state, it exhibits low ductility. The present work is an extension of our earlier effort to improve the processability and mechanical properties of PLA by blending with poly[(butylene succinate)-*co*-adipate)] (PBSA), a biodegradable polymer with lower glass transition temperature. We evaluate the influences of incorporation of an epoxy chain extender and nanoclay on the properties of the blend. Since earlier work was conducted in a batch mixer, the influence of melt processing in the twin screw extruder and the differences between products obtained in the extruder and the batch mixer are evaluated and explained. Based on earlier work, the following PLA/PBSA blend ratios of 90:10, 80:20 and 70:30 were selected. All the samples were prepared in the twin-screw extruder at two different screw speeds (50 and 150 rpm), to evaluate the effects of residence time and shear rates. The morphology and structure of the blends were examined using field emission scanning electron microscopy. Transmission electron microscopy (TEM) and X-ray diffraction (XRD) were used to evaluate the levels of intercalation and exfoliation in the nanocomposites. The chain extension reaction was evaluated using nuclear magnetic resonance (NMR) spectroscopy and other techniques. Rheological properties (dynamic oscillatory shear and elongational viscosity measurements) and mechanical characteristics of the pure components, blends, and nanocomposites were studied and discussed in light of the composition and morphology of the blends and the nanocomposites. © 2015 Wiley Periodicals, Inc. J. Appl. Polym. Sci. **2015**, *132*, 42664.

KEYWORDS: biodegradable; morphology; rheology

Received 13 April 2015; accepted 29 June 2015
DOI: 10.1002/app.42664

INTRODUCTION

Different approaches have been considered to improve the brittle behavior and low melt strength of biodegradable poly (lactic acid) (PLA) and to extend its fields of application.[1–5] For example, the chain extension reaction was considered as valuable solution to increase the elongational melt properties where strain-hardening occurred for modified PLAs with an epoxy-based chain extender.[6] Preparation of polymer blends using poly(butylene succinate-*co*-adipate) (PBSA) and poly (butylene adipate-*co*-terephthalate) (PBAT) to improve both mechanical and rheological properties was also studied.[7,8] In earlier work, using the internal batch mixer, we evaluated the effects of (i) blending PLA with PBSA and (ii) the addition of an epoxy-based chain extender on rheological and mechanical properties of the corresponding blends.[9,10] The results of these studies indicated significant improvements in melt strength over that of PLA, which makes such systems more suitable for some polymer processing operations (e.g., film blowing, blow molding, and fiber spinning). However, over 50 wt % PBSA was required in the first approach. Such large PBSA content produced PLA/PBSA blends with high ductility, even in the presence of clay.[11] On the other hand, it was found that blending in the presence of a chain extender for 15–20 minutes enhances both the ductility and melt strength of PLA systems, even at 30 wt % PBSA.[10] While the above work in the batch mixer has produced significant results, it is still necessary to test some of these findings using more likely commercial processing systems. Since it is expected that commercial production of the above blends and nanocomposites would more likely involve melt extrusion, it is necessary to evaluate the effects of the chain extension reaction in the extruder, with shorter residence times and higher shear rates.

Table I. Some Characteristics of the Pure Components

Properties	PLA (4032D)	PBSA (3001M)	ASTM method
Density (g/cm^3)	1.24	1.23	D792
Glass transition Temp. (°C)	55-60	−45	D3418
MFR (g/10 min) *210°C/2.16kg	7	1.4	D1238
Peak melt Temperature (°C)	155-170	94	D3418

In other work, rheological evaluation of PLA/PBSA/nanoclay ternary nanocomposites prepared using an internal batch mixer showed that significant strain-hardening behavior was observed only for nanocomposite prepared at high PBSA content.[12] Moreover, the elongational viscosities of the blends were lower than those of corresponding nanocomposites at small Hencky strain. However, the inverse relative rheological behavior was observed at larger Hencky strain, possibly due to destruction of the network-like structure of clay.[12] It was suggested that the oriented clay platelets lead to the lower elongational viscosity for the ternary nanocomposites. Analysis of the interfacial energy data for the nanocomposites, indicated that clay platelets should be preferentially located at the PLA/PBSA phase interface, with small amounts of clay located within the PLA and PBSA phases.[12]

It should be pointed out that recent reports regarding PLA systems, investigated the blending of non-reactive components and/or the processing of reactive systems in internal batch-mixers. Therefore, more studies are needed to obtain better insight into the behavior and effect of chain extenders in reactive extrusion.

The present work evaluates the processing behavior and mechanical properties of PLA systems produced using a combination of the three above approaches (blending with PBSA, chain extension reaction & incorporation of nanoclay) in reactive extrusion. The chain extension reaction of the prepared blends and corresponding nanocomposites are characterized using different criteria, such as acid values, material functions in rheological analysis, nuclear magnetic resonance (NMR) signal line width and end-group analysis. The combination of the above analyses appears to be sufficient to provide a clear description of the products.

EXPERIMENTAL

Materials and Preparation of Blends and Nanocomposites

PLA 4032D (Natureworks, LLC) was used in this study. Synthetic biodegradable PBSA (Bionolle 3001*M*) was supplied by Showa High Polymer, Japan. Some characteristics of the relevant grades are presented in Table I as reported by the suppliers. An additive based on epoxy-functionalized PLA (CESA Extend OMAN698493), hereafter called CESA, was used as chain extender. Cloisite 30B (Southern Clay products, U.S.A), organically modified montmorillonite nanoclay with methyl, tallow, bis(2-hydroxyeethyl) quaternary ammonium chloride, was used. Cation-exchange capacity (CEC) and X-ray diffraction *d*-Spacing (001) of Cloisite 30B are 90 (meq/ 100g clay) and 18.5 Angstroms, respectively, as reported by the supplier. All materials (PLA, PBSA, and C30B) were dried under vacuum at 60°C for 72 hours prior to processing.

Extrusion was performed using a Leistritz 18 HP co-rotating twin screw extruder (D =18 mm, L/D = 40) equipped with eight controllable heating zones. Blends of PLA and PBSA with different PLA/PBSA ratios (90:10, 80:20, 70:30) were prepared at a single CESA concentration (2 wt % based on PLA content). Firstly, granules of PLA and PBSA were hand-mixed in a plastic container. For the preparation of the nanocomposites, a master-batch containing 15 wt % Cloisite 30B, based on PLA, was prepared using the same twin screw extruder. The efficacy of the masterbatch approach to improve dispersion and to increase the degrees of exfoliation of nanoclay, tensile strength and modulus, in comparison with the direct mixing process, was reported in the literature.[13] The prepared master-batch was then used to prepare nanocomposites based on PLA/PBSA blends at a single clay concentration (3 wt %), using the twin screw extruder. All extrusion operations were carried out at two screw speeds (50 rpm, residence time of $\sim$ 150 s and 150 rpm, residence time of $\sim$ 90 s). The temperature distribution in the extruder was maintained at (from the feeder to the die): 170, 175, 175, 180, 180, 180, 180, 175°C. Also, PLA and PLA with 2 wt % chain extender were processed under the same processing conditions. Blends and nanocomposites were designated as CPLAxxyyy and CNPLAxxyyy respectively, where xx (first two digits) indicates the PLA weight percent, and yy is the screw speed (Table II).

Table II. Composition and Nomenclature of the Samples

PLA/ PBSA ratio	Nanoclay (wt %)	CESA based on PLA content (wt %)	Screw speed (rpm)	Nomenclature
100:0	0	0	50	PLA50
100:0	0	0	150	PLA150
100:0	0	2	50	CPLA50
100:0	0	2	150	CPLA150
90:10	0	2	50	CPLA9050
90:10	0	2	150	CPLA90150
80:20	0	2	50	CPLA8050
80:20	0	2	150	CPLA80150
70:30	0	2	50	CPLA7050
70:30	0	2	150	CPLA70150
90:10	3	2	50	CNPLA9050
90:10	3	2	150	CNPLA90150
80:20	3	2	50	CNPLA8050
80:20	3	2	150	CNPLA80150
70:30	3	2	50	CNPLA7050
70:30	3	2	150	CNPLA70150

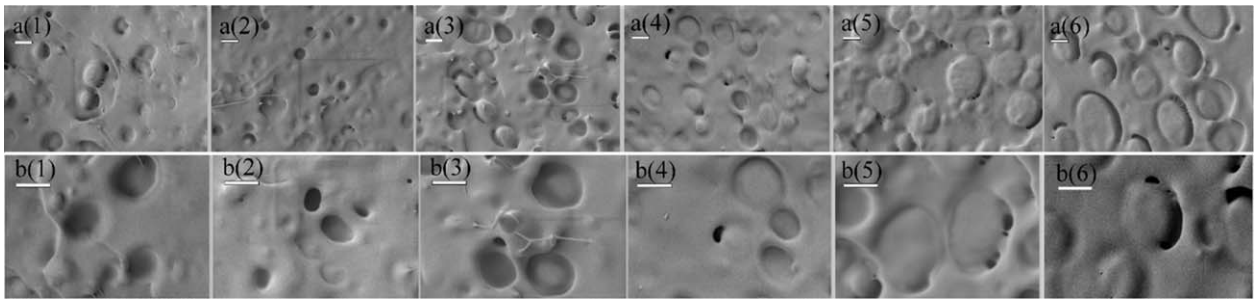

Figure 1. SEM micrographs of (1) CPLA90150; (2) CPLA9050 ; (3) CPLA80150; (4) CPLA8050; (5) CPLA70150; (6) CPLA7050 at two different magnification (a) 10,000× and (b) 20,000× (The scale bar is 1 μm).

Characterization Methods

XRD was carried out at room temperature with an X-ray diffractomer (Philips model X'PER). The X-ray source was Cu-Ka radiation (λ= 1.540598 angstroms) using a 50 kV voltage generator and 40 mA current. The angular step size was 0.02° with a step time of 1 second from 1° to 10°. The samples for scanning electron microscopy (SEM) were obtained by fracture in liquid nitrogen. The fractured samples were coated with gold/palladium by plasma deposition for a period of 20 seconds. The morphology of the blends was evaluated using field emission scanning electron microscopy (JEOL) operated at 1.5 kV. To calculate the acid value, around 3 g of the sample were dissolved in 60 mL of $CHCl_3$ to prepare the solution.

For transmission electron microscopy (TEM), PLA/PBSA/Cloisite 30B nanocomposites were trimmed to prepare a truncated pyramid section with a razor blade, to avoid the high pressure on the diamond knife. Then, they were ultra-microtomed at −70°C (sample temperature) using a Reichert/Leica Ultra microtome to prepare samples with thickness of ∼30 to ∼50 nm. A cryo wet 35° knife with DMSO/water bath was used to transfer the sections to 200-mesh copper grids. TEM micrographs were taken with Jeol JEM-2100F and recorded with a digital camera.

The surface energy was evaluated using sessile drop measurements at room temperature to determine contact angles. Clay and polymer granules were dried in vacuum oven at 80°C overnight and at 60°C for 4 h; respectively. The device description and the method details can be found elsewhere.[14,15]

Titration was carried out using a solution of KOH in MeOH with a concentration of 2 .03 × 10^{-2} mol L^{-1} using phenolphthalein as the indicator. The equivalent volume V_e was used to determine the acid value by the following equation (6):[6]

$$\mathrm{AV} = \frac{V_e \times C(\mathrm{KOH}) \times M(\mathrm{KOH})}{m\,(\mathrm{Polymer})} \qquad (1)$$

where AV is the acid value, V_e is the equivalent volume required to reach the equilibrium pH, C (KOH) is the molar concentration of KOH, M (KOH) is the molar mass of KOH and m is the weight of dissolved polymer. The results are reported in milligrams (KOH) per gram (polymer). ^{1}H NMR spectra were performed using a Bruker spectrometer operating at 500 MHz with chemical shifts referenced to tetramethylsilane at room temperature. Samples were dissolved in a chloroform-d solution ($CDCl_3$). The resonance signals at different chemical shifts (δ), expressed in ppm were assigned to the different protons according to the available literature.[16,17]

All the samples were prepared for rheological and mechanical measurements, using a Carver press operated at 5 MPa and 180°C for a period of 9 min heating (5 min preheating, 4 min heating under pressure) and 5 min cooling under pressure. A stress-controlled rheometer (Physica MCR 301, Anton Paar) with parallel plate configuration was used to perform small amplitude oscillatory shear (SAOS) measurements over a frequency range from 0.1 to 100 rad/s at 180°C. The gap was adjusted to 1.2 mm. The elongational viscosity was measured using a SER Universal Testing Platform in combination with ARES (Rheometrics Scientific) rheometer at 180°C. Dumbbell shape specimens for tensile tests (according to ASTM-D 638) were molded as described above. The tensile tests were conducted using an MTS universal tensile testing machine. A crosshead speed of 1 mm/min was set for all tests.

RESULTS AND DISCUSSION

Morphology of the Blends and Clay Dispersion

Figure 1 shows the SEM images of the fractured surfaces of PLA/PBSA blends with chain extender at different PLA/PBSA ratio, prepared at screw speeds of 50 rpm and 150 rpm. At low PBSA content, the PBSA droplets become smaller and more uniform. Although it is difficult to infer the real blend morphology using two-dimensional images, the number average diameter (D_n) and the volume average diameter (D_v), were estimated using a digitizing table and user-defined transformer file.[18] (D_n, D_v) for CPLA90150, CPLA80150 and CPLA70150 were calculated to be (0.84 μm, 0.91 μm), (1.23 μm, 1.28 μm) and (1.94 μm, 2.10 μm), respectively, in comparison with the values of (0.45 μm, 0.47 μm), (1.04 μm, 1.1 μm) and (1.88 μm, 1.99 μm) for the corresponding blends prepared with lower screw speed (50 rpm). The mean diameter of the droplets becomes smaller for samples prepared at lower screw speed. It is suggested that the breakup of highly elongated threads via capillary instabilities leads to a line of smaller droplets. When the thread wavelength is greater than 2πr (r being the thread radius), breakup occurs, if the residence time during the mixing process is longer than the breakup time.[19] The breakup time is obtained by:

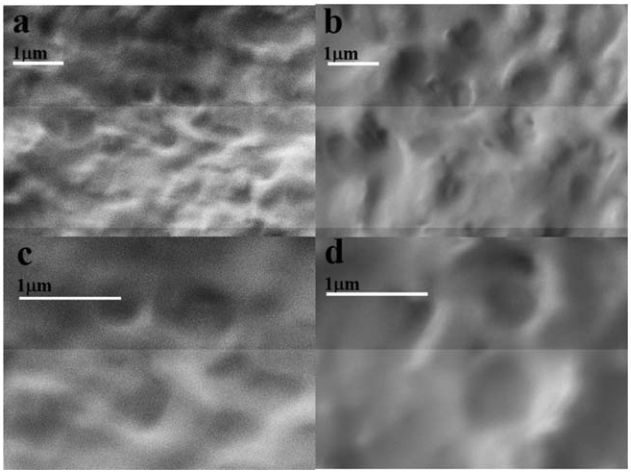

Figure 2. SEM micrographs of (a, c) CNPLA80150; (b) CNPLA70150; (d) CNPLA8050; at two different magnification 20,000× and 40,000× (The scale bar is 1 μm).

$$t_b = \left(\frac{\eta_m B}{\Omega(l,\lambda)\sigma}\right) \ln\left(\frac{0.8B}{2\alpha_0}\right) \tag{2}$$

where η_m is the matrix viscosity, B is the diameter of the elongated thread, σ is the interfacial tension, α_0 is the amplitude of the initial distortion and $\Omega(l,\lambda)$ is the Tomokita function depending on the distortion wavelength l and the viscosity ratio λ. High matrix viscosity should lead to long breakup times, but this term is already included in $\Omega(l,\lambda)$, which increases with decreasing viscosity ratio.[19] If one assumes affine deformation, then a reduction in the total amount of imposed strain causes an increase in the diameter of the elongated thread (B). On the other hand, higher viscosity of the matrix, due to the higher extent of chain extension reaction for the blends prepared at lower screw speed, as shown in the following section, would lead to longer breakup times and thinner elongated threads of the PBSA before breakup. Consequently, lower droplet size would be obtained at lower screw speed, compared to the droplet size of PLA/PBSA blends prepared at higher screw speed. Figure 2 shows that incorporation of nanoclay in the blends caused a significant reduction in the droplet size, in comparison with the corresponding blends. The PBSA droplet size increased by increasing PBSA content [Compare Figure 2(a,b)]. Also, decreasing the screw speed caused an increase in PBSA droplet size for the nanocomposites, which is opposite to the trend observed for the blends [Compare Figure 2(c,d)].

XRD analysis was performed on Cloisite 30B and the nanocomposites. Basal spacing values were calculated from the value of θ (the scattering angle) and λ (the wavelength of incident wave) using Bragg equation [$2d\mathrm{Sin}(\theta) = n\lambda$] where n is a positive integer. The characteristic peak of Cloisite 30B shown in Figure 3(a) corresponds to ~1.8 nm basal spacing (d_{001}). The XRD patterns for the nanocomposites show a change in d-spacing from ~1.8 to ~4.0 nm. The larger basal spacing of clay in comparison with the virgin Cloisite 30B suggests intercalation by the polymer chains. The results shown in Figure 3 demonstrate that the degree of intercalation depends slightly on both the screw speed and PBSA content, since the intensity of the peak at $2\theta = 2.25°$ and $2\theta = 4.7°$ decreased at higher screw speed [Figure 3(b,c)] and higher PBSA content [Figure 3(b,d)].

TEM images shown in Figure 4 confirm the existence of intercalated dispersed tactoids containing small numbers of clay layers. These tactoids are well dispersed and separated from each other.

Localization of the Clay

The selective localization of the nanoclay influences not only the rheological and mechanical behavior of the nanocomposite but also the reactions of the chain extender. The wetting coefficient (ω_a) determines the location of the clay in the ternary system. It depends on the interfacial energies (γ_{ij}) for the three pairs associated with the three component system, where i or j is Polymer A, Polymer B, or clay according to the following relationship:[20–22]

$$\omega_a = \frac{\gamma_{\text{Nanoclay -PolymerB}} - \gamma_{\text{Nanoclay -PolymerA}}}{\gamma_{\text{PolymerA-PolymerB}}} \tag{3}$$

The filler is located in Polymer A when the wetting coefficient is higher than 1 ($\omega_a > 1$). The filler is located in Polymer B, if the wetting coefficient is lower than −1 ($\omega_a < -1$). If the wetting coefficient is between 1 and −1 ($-1 < \omega_a < 1$), the filler is mainly located at the interface between the two blend components.[20–22] The surface energies (γ_i) were determined according to Good & Van Oss model.[23,24]

$$\gamma_i = \gamma_i^{\,d} + \gamma_i^{\,p} = \gamma_i^{\,d} + 2\sqrt{\gamma_i^{\,+}\gamma_i^{\,-}} \tag{4}$$

where γ_i^d is the dispersive component of the surface energy (Lifshitz-Van der Waals interactions), γ_i^+ is the electron–acceptor (Lewis acid) parameter and γ_i^- is the electron–donor (Lewis base) parameters of the polar component (γ_i^p). The above surface energy components were calculated using the contact angle (θ) values as obtained from the sessile drop experiments and the values of the surface tension of the used liquids (Table III) according to the following relation:

$$\gamma_1(1+\cos\theta) = 2\left(\sqrt{\gamma_i^{\,d}\gamma_1^{\,d}} + \sqrt{\gamma_i^{\,+}\gamma_1^{\,-}} + \sqrt{\gamma_1^{\,+}\gamma_i^{\,-}}\right) \tag{5}$$

where γ_l is the surface tension of the liquid. The results are summarized in Table IV.

Based on the values of the surface energies for PLA, CPLA150, PBSA, and Cloisite 30B, the interfacial energies (γ_{ij}) for pairs of PLA/PBSA, CPLA150/PBSA, PLA/Cloisite 30B, CPLA150/Cloisite 30B and PBSA/Cloisite 30B were determined using the geometric-mean equation as follows:

$$\gamma_{ij} = \gamma_i + \gamma_j - 2\left[(\gamma_i^d\gamma_j^d)^{\frac{1}{2}} + (\gamma_i^p\gamma_j^p)^{\frac{1}{2}}\right] \tag{6}$$

The wetting coefficient was then estimated using the data presented in Table V. The calculated wetting coefficients for PLA/PBSA/Cloisite 30B and CPLA150/PBSA/Cloisite 30B ternary nanocomposites are about −0.99 and −0.71, respectively. These values imply that clay platelets are preferentially located at the phase interface, with small amounts located within the PLA and PBSA phases. The literature values of the surface energies of PLA,[9,26,27] PBSA,[15] and Cloisite 30B[28,29] led to the wetting coefficient of −0.72. The surface energy values at processing temperature were extrapolated from the experimental data at room

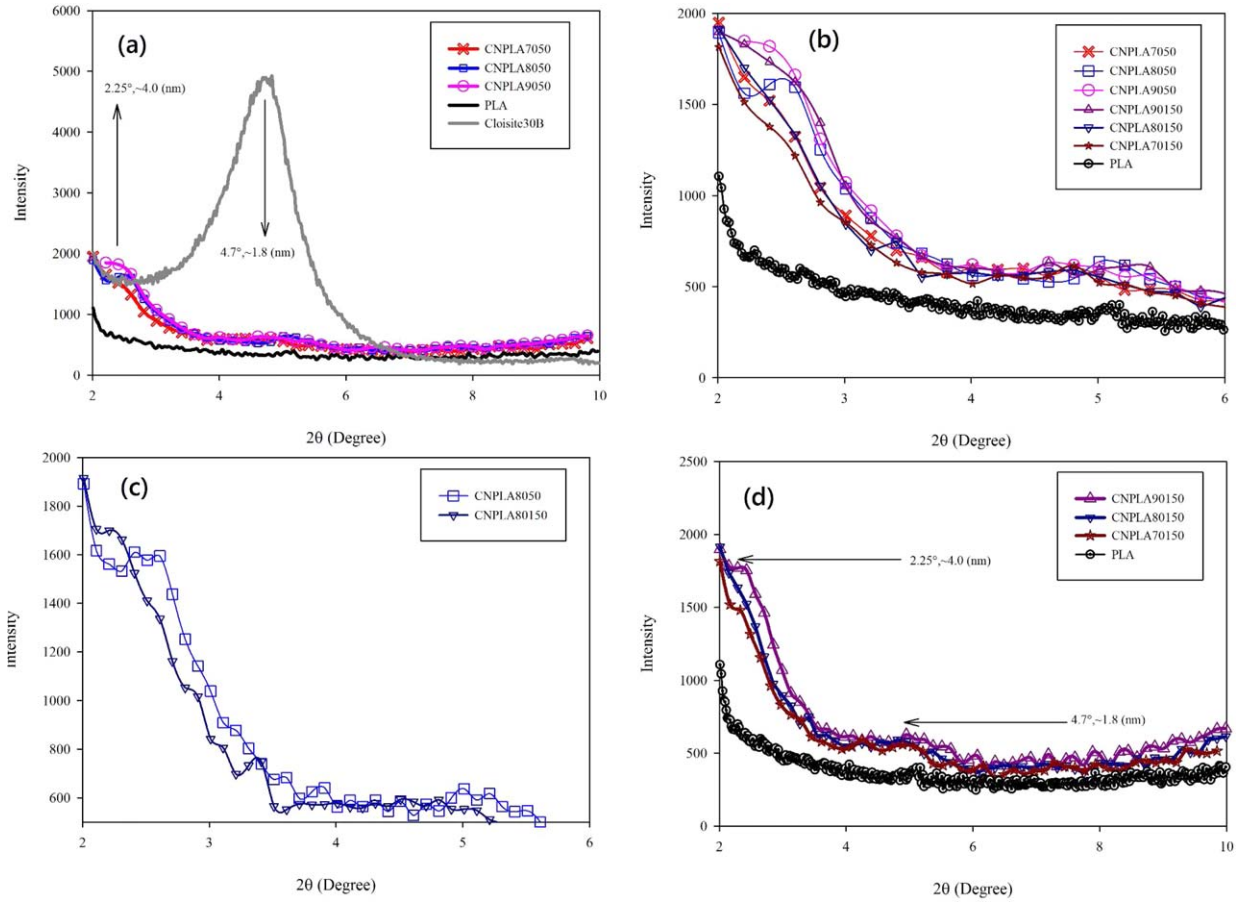

Figure 3. XRD patterns of Cloisite 30B and PLA/PBSA nanocomposites. [Color figure can be viewed in the online issue, which is available at wileyonlinelibrary.com.]

temperature (using temperature coefficient of −0.06 (mN/m K).[26] The estimated value of the wetting coefficient at processing temperature is −0.37. TEM micrographs in Figure 4 support this prediction and show that the PBSA droplets are surrounded by nanoclay.

Chain Extension and Degradation Reactions

The epoxy chain extender reacts with the polyester carboxyl group.[6] Therefore, the determination of the acid value could be an appropriate indicator of the extent of the chain extension reaction. Figure 5 shows the acid values measured for neat and chain extended PLAs extruded at 50 rpm and 150 rpm screw speed. It should be noted that the higher acid values of nanocomposites as compared to their corresponding blends is related to the presence of the modifier in Cloisite30B.[30] The results in Figure 5 show that increasing the screw speed for the neat PLA leads to an increase in the acid value, due to PLA degradation and chain scission, which produces new carboxyl groups. In the

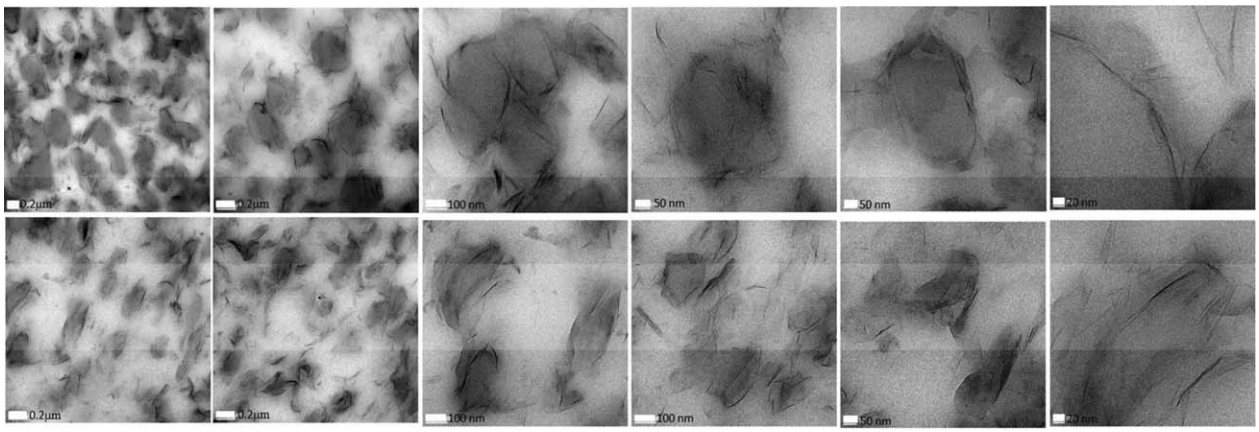

Figure 4. TEM micrographs of CNPLA70150 (first row) and CNPLA90150 (second row) at different magnification.

Table III. Surface Energy Components (mN/m) of the Used Liquids in the Sessile Drop Experiments[25]

Material	γ_l	γ_l^d	γ_l^p	γ_l^+	γ_l^-
Water	72.8	21.8	51.0	25.5	25.5
Glycerol	64	34	30	3.92	57.4
Diiodomethane	50.8	50.8	0.0	0.0	0.0

presence of chain extender, increasing the screw speed leads to considerable reduction in acid value, as a result of the competition between chain scission and chain extension. The same effect of increasing screw speed was also observed for the acid values of CNPLA80 and CNPLA70 series of samples. However, acid values of CPLA8050 and CPLA7050 were lower than those of CPLA80150 and CPLA70150. Thus, at higher PBSA content levels, the local concentration of chain extender in the PLA phase decreases. Consequently, the residence time becomes a more important factor, compared to the thermo-mechanical effect of screw speed. On the other hand, clay platelets located at the phase interface (Figure 4) limit the diffusion of the chain extender to the PBSA phase and increase its local concentration in PLA. The results of ^{1}H NMR spectroscopy, shown in Figure 6, support this conclusion. It should be noted that all the blends were completely soluble in $CHCl_3$ during the acid value measurements. It shows that crosslinking has not taken place to form a three dimensional network and chain extension reaction has not led to such complex structure.

All the NMR spectra showed two resonance peaks at 5.19 ppm denoted by (a) and 1.61 ppm denoted by (b), which are attributed to methine (CH) and methyl (CH_3) protons of repeat units of PLA (Table VI). The ratio of the integrated peak intensities is equal to 1:3.03, as expected from theory. The HNMR spectra of PLA also show resonance signals at 4.38 and 2.6 ppm, assigned to the methine protons next to the hydroxyl end-group (c) and the methine protons next to the terminal carboxylic group (e), respectively. The resonance peak at 1.05 ppm (d) is considered to belong to methyl protons close to terminal hydroxylic groups. The resonance peak observed at 4.12 ppm is attributed to the proton in terminal hydroxylic group, and it is denoted here as (g). The integration ratios between the (a) and (c) peaks for the CPLA50, CPLA150 and PLA150 are 10,000:7, 10,000:6 and 10,000:7, respectively. It seems that by increasing the screw speed, the number of hydroxyl ends decreases slightly compared to the samples prepared at lower screw speed, because of their reaction with the chain extender.

Table V. Interfacial Energies Calculated from the Geometric-Mean Equation

Sample A	Sample B	Interfacial energy (mN/m)
PLA	PBSA	1.10
CPLA150	PBSA	1.56
PLA	Cloisite 30B	0.58
CPLA150	Cloisite 30B	0.54
PBSA	Cloisite 30B	1.67

The same trend was also observed based on the analysis of the integration ratios between the (a) and (g) peaks. On the other hand, the integration ratios between the (a) and the (e) peaks are 10,000:6, 10,000:4 and 10,000:9 for CPLA50, CPLA150 and PLA150, respectively. For the neat PLA, the integration ratio between the (a) and the (c) peaks is approximately equal to the ratio between the (a) peak and the (e) peaks (i.e., 10,000:7). Based on these integration calculations, it appears that the epoxy-based chain extender is more reactive towards the terminal carboxylic group. Also, the formation of the new carboxyl groups due to the thermal degradation at high screw speed compared to neat PLA is clear. The significant increase in the integration ratio between the (a) and the (e) peaks for the CPLA70150 (10,000:62) can be attributed to the shear heating due to the high viscosity of PBSA phase, which leads to a higher degree of thermal degradation of the PLA phase.

The broad backbone peaks for the nanocomposite do not allow us to conduct end-group analyses. However, it is known that the mobility of a polymer segment is directly related to its signal width. A decrease in segmental mobility due to the increase in molecular weight broadens the observed segment signal. Therefore, as seen in Figure 6, the higher backbone peak base width for the nanocomposite (CNPLA70150) as compared to CPLA70150 suggests a more advanced chain extension reaction. This is in agreement with our rheological results as discussed in the next section.

Rheological Behavior Under Shear

The effects of reactive extrusion and nanoclay presence on the rheological properties of PLA/PBSA systems were evaluated using SAOS experiments. First, to ensure that oscillatory shear measurements are conducted within the linear regime, strain sweep experiments were performed. Theoretically, the strain limit at low frequency should also apply at high frequency. The high resolution of the instrument assured the accuracy of measurements, when a strain amplitude of 3% was used for all the

Table IV. Contact Angle Measurements and Surface Energies

	Contact angle (θ)			Surface energy (mN/m)		
Sample name	Water	Diiodomethane	Glycerol	γ_s^d	γ_s^p	γ_s
PLA	71° ± 1.2	46.8° ± 0.6	62.47° ± 1.2	36.03	4.57	40.60
CPLA150	72.03° ± 1.1	50.12° ± 0.5	62.9° ± 1.5	34.20	5.18	39.39
PBSA	68.46° ± 0.5	32.26° ± 1.9	61.9° ± 1.1	43.26	7.1	50.36
Cloisite 30B	79.4° ± 0.6	59.6° ± 0.5	73.6° ± 1.2	28.80	2.95	31.75

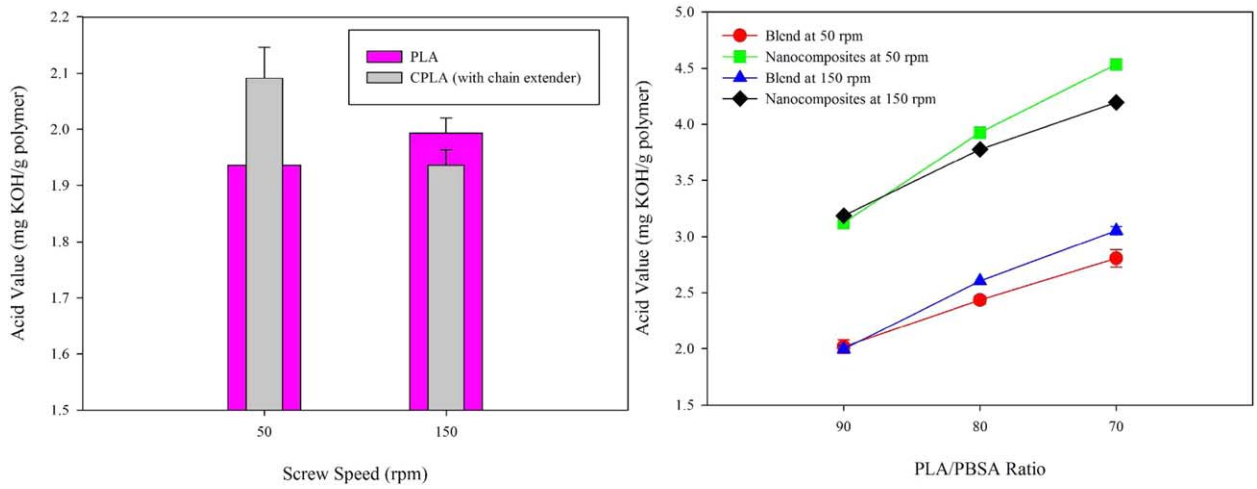

Figure 5. (a) Acid values of neat PLA, CPLA; (b) PLA/PBSA blends and their nanocomposites with Chain extender. [Color figure can be viewed in the online issue, which is available at wileyonlinelibrary.com.]

samples to guarantee the linearity. It should be mentioned that the critical strain for the pure components is about 10% at angular frequency of 1 rad/s.

Figure 7(a) shows that PLA50 and PLA150 exhibit a Newtonian plateau at low frequency. Increasing the screw speed leads to a reduction in the complex viscosity of PLA due to thermal degradation. The Newtonian plateau is also observed for CPLA50 and CPLA150. The latter showed significantly higher zero shear viscosity, and transition from the Newtonian plateau to the shear-thinning regime shifted to lower angular frequency. These results confirm the role of the competition between chain scission and chain extension as indicated by the extent of reaction measurements [Figures 5(a) and 6(a)]. Pure PBSA showed higher complex viscosity (η^*) at low angular frequency (ω), compared to the PLAs and CPLAs. The difference between complex viscosity of PBSA and CPLA150 becomes negligible at high ω.

Figure 7(b,c) show that the blends and their corresponding nanocomposites do not exhibit a Newtonian plateau, at least in the experimental window considered. Structural changes in polymeric systems can be traced with the linear viscoelastic properties, especially in the terminal region. In fact, SAOS measurements are very sensitive to the topological structure of macromolecular chains at low frequencies, where significant connections between the rheology and structure can be made. Figure 7(b,c) suggest the presence of microstructure with long relaxation time due to the chain extension reaction. However, a part of non-Newtonian behavior could be related to the structure and morphology of the blends and nanocomposites. SAOS measurements of blends and nanocomposites point out two trends that should be considered: (*i*) η^* values of the nanocomposites with chain extender prepared at higher screw speed (150 rpm, residence time of ~90 s) were greater than those of corresponding nanocomposite prepared at lower screw speed (50 rpm, residence time of 150s), and (*ii*) η^* increased by raising the PBSA content in the nanocomposites. However, these trends were not observed for the blends. In comparison with the corresponding samples prepared in the internal batch mixer,

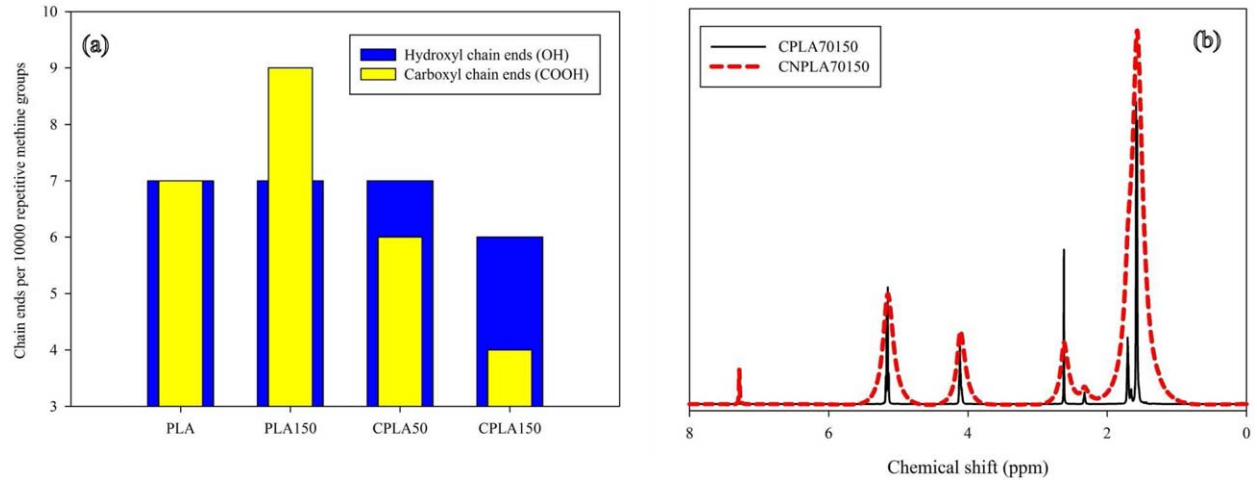

Figure 6. (a) The extent of reaction in terms of number of hydroxyl and carboxyl chain ends, (b) ^{1}H-NMR spectra of CNPLA70150 and CPLA70150. [Color figure can be viewed in the online issue, which is available at wileyonlinelibrary.com.]

Table VI. Peak Assignment of ^{1}H NMR Spectra of PLA[17]

Chemical shift (ppm)	Type of proton	Designated name
5.19	The methine (CH) protons of repeat units of PLA	(a)
1.61	The methyl (CH3) protons of repeat units of PLA	(b)
4.38	The methine protons next to the hydroxyl end-group	(c)
1.05	The methyl protons close to terminal hydroxylic groups.	(d)
2.6	The methine protons next to the terminal carboxylic group	(e)

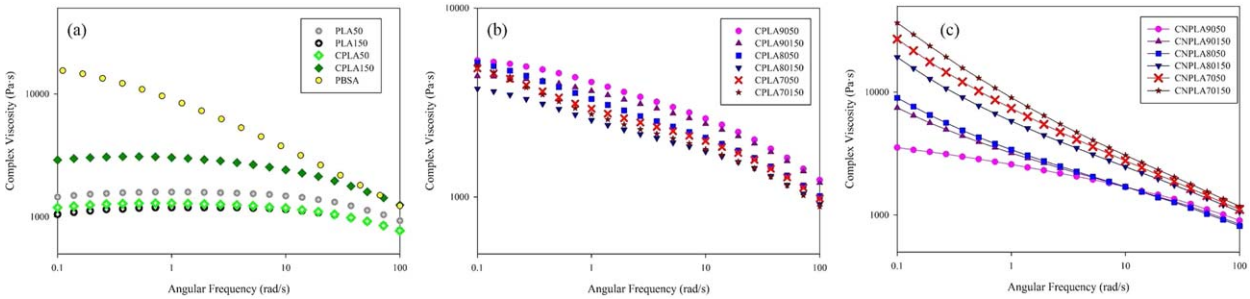

Figure 7. Complex viscosity of the (a) PLA and CPLA (b) PLA/PBSA blends and (c) PLA/PBSA nanocomposites. [Color figure can be viewed in the online issue, which is available at wileyonlinelibrary.com.]

η^* of the blends increases upon raising the PBSA.[10,31] This difference may be attributed to the fact that the residence time in reactive extrusion is shorter than that in the internal batch mixer. Thus, upon increasing the PBSA content, a certain amount of the chain extender is mixed into the PBSA phase, but this amount does not have enough time to diffuse back into the PLA matrix in the time frame of the extrusion process. This effect is more pronounced at higher screw speed. Consequently, the contribution of chain extender to modification of the rheological properties becomes smaller than in the case of the samples prepared in the internal batch mixer. In the case of nanocomposite, as indicated above, the PBSA phase is surrounded by naonoclay layers/tactoids (Figure 4). This limits the diffusion of the chain extender into the PBSA phase and leads to a higher extent of the chain extension reaction with PLA. Moreover, the lower residence time in the extruder favors the chain extension reaction in competition with thermal degradation. Therefore, the nanocomposites would be expected to exhibit higher complex viscosity compared to the corresponding blends, either due to the reinforcing effect of nanoparticles and/or due to the effect on chain extension reaction. Figure 8 shows the results for storage modulus (G'), as a measure of the elasticity of the prepared samples. It provides a sensitive indication of the structural changes that take place in polymer compounds. The elastic modulus of the blends was higher than that of PLA with or without chain extender in the low-ω region. Also, it increased slightly with increasing PBSA content. G' values for the nanocomposites were higher than those for the corresponding blends, and the difference was more pronounced for the system with higher PBSA content. Opposite to the trend observed

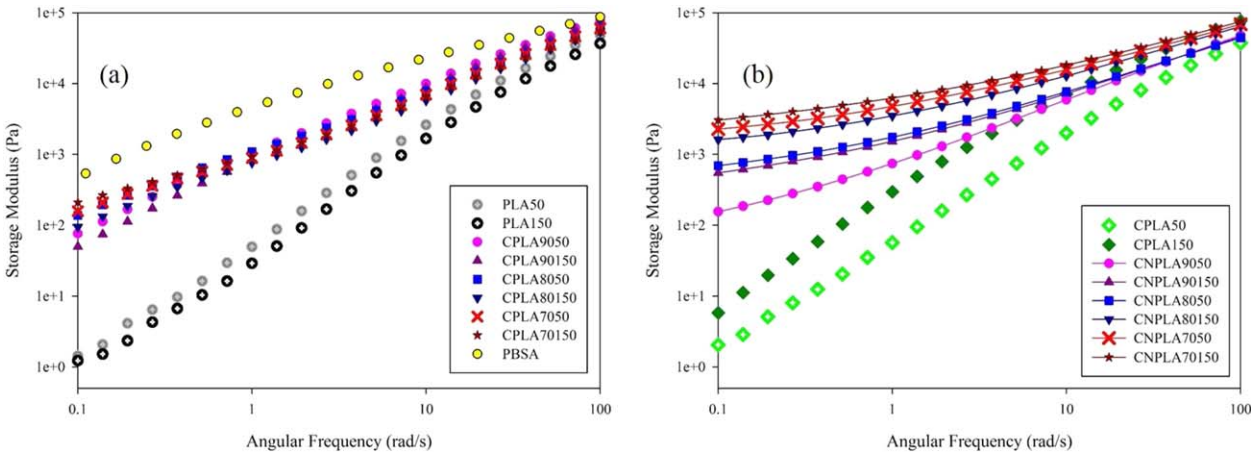

Figure 8. Storage modulus of the (a) pure component and PLA/PBSA blends and (b) chain extended PLA and PLA/PBSA nanocomposites. [Color figure can be viewed in the online issue, which is available at wileyonlinelibrary.com.]

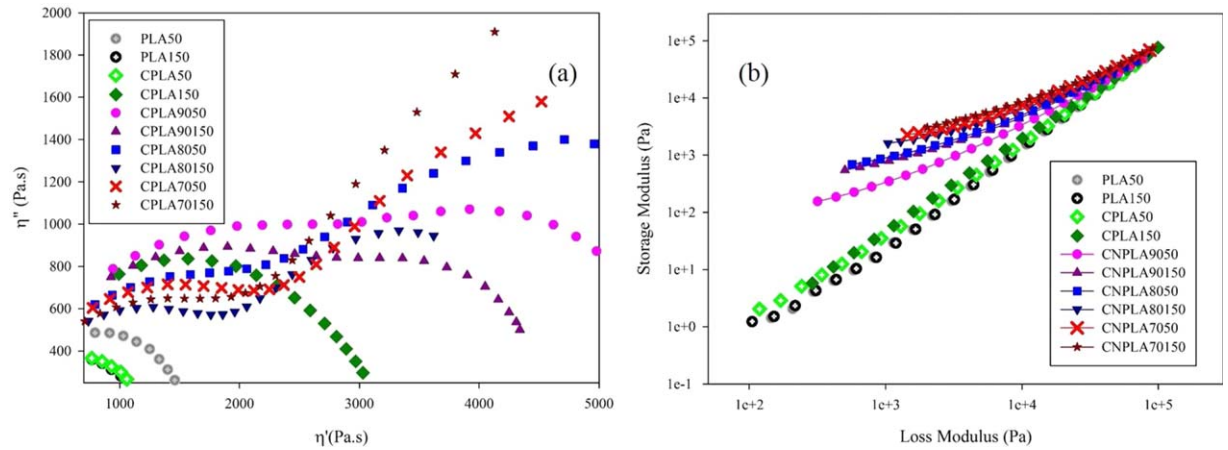

Figure 9. (a) Cole–Cole plot and (b) modified Cole–Cole plot of the pure component, PLA/PBSA blends and nanocomposites. [Color figure can be viewed in the online issue, which is available at wileyonlinelibrary.com.]

for the blends, G' for the nanocomposites increased by increasing the screw speed (Figure 8).

All the compounds deviated from terminal behavior of the linear polymer (i.e., $G' \propto \omega^2$ & $G'' \propto \omega$). This can be associated with changes in the structure and morphology of the samples. The structural changes due to the chain extension reaction could also be tracked by the Cole–Cole plot (the curve of η'', the out-of-phase component of complex viscosity vs. η', the dynamic viscosity) and the modified Cole–Cole plot (the curve

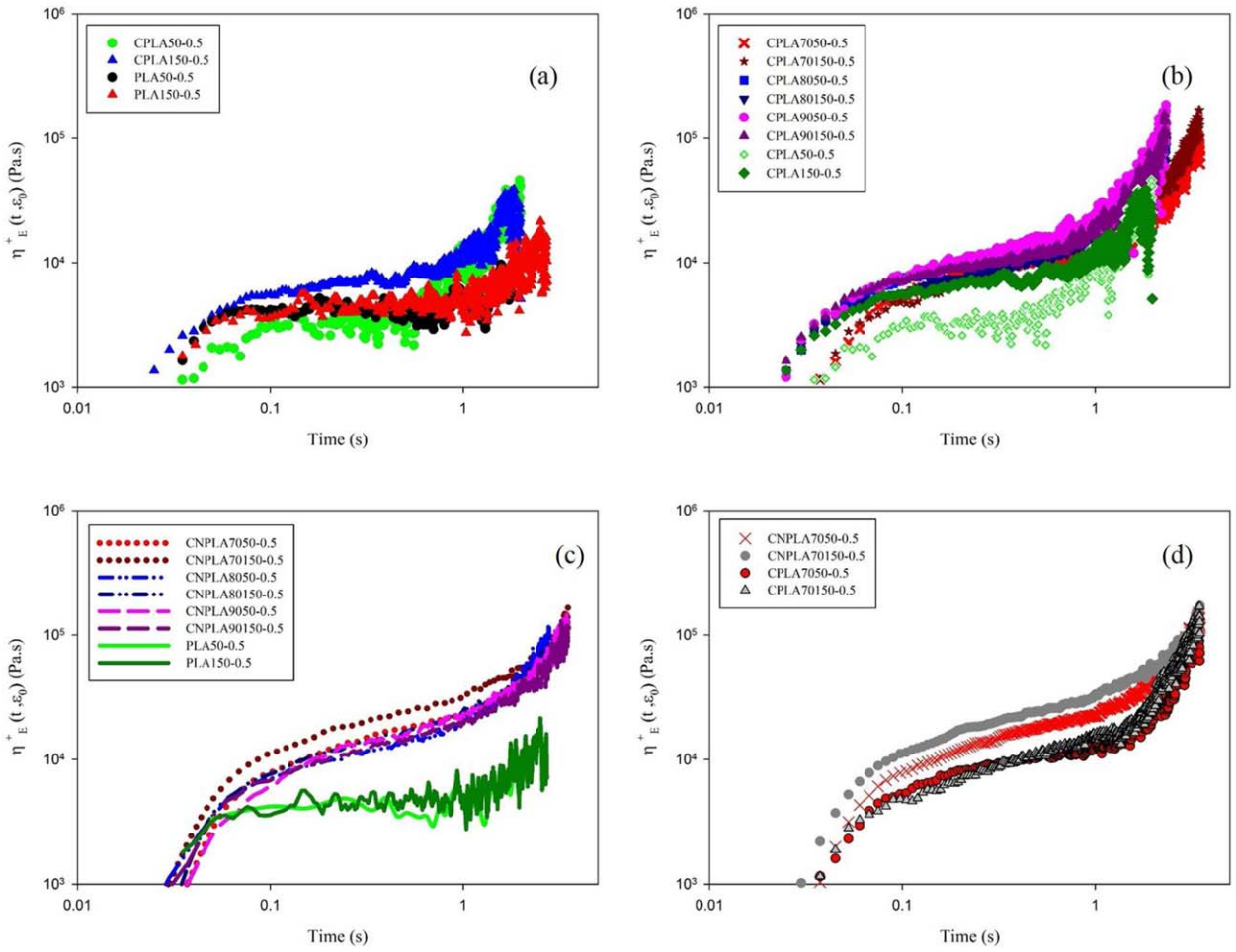

Figure 10. Elongational viscosity values for different PLA systems, PLA/PBSA blends and their nanocomposites. [Color figure can be viewed in the online issue, which is available at wileyonlinelibrary.com.]

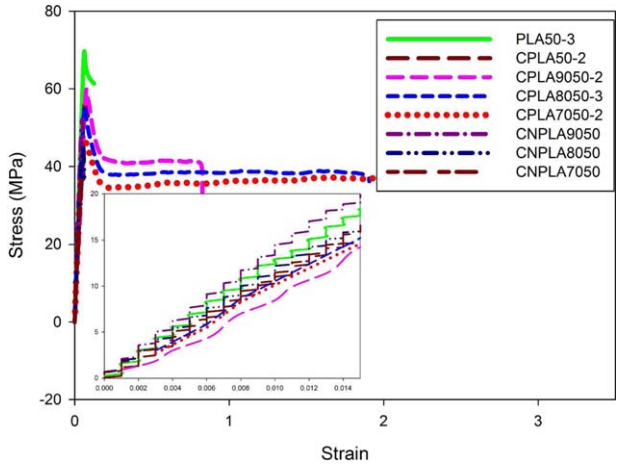

Figure 11. Stress–strain curve of the PLA systems, PLA/PBSA blends and their nanocomposites. [Color figure can be viewed in the online issue, which is available at wileyonlinelibrary.com.]

of log G' vs. log G'') at a constant temperature.[32] Figure 9(a) shows a concave Cole–Cole curve close to a semicircle for Pure PLAs. The Cole–Cole plots of the prepared blends deviated from the semicircular shape due to the long relaxation time. The deviation from the semicircular shape was more obvious for nanocomposites (data not shown) with chain extender than for PLA with chain extender. The extent of this deviation was related to the extent of chain extension reaction and microstructure of the blends and nanocomposites, as indicated above.

Nonlinear behavior is clearly observed in the modified Cole–Cole plots of all the blends and nanocomposites. The deviation from the terminal relation ($G' \propto G''^2$) could be related to the immiscibility of the PLA and PBSA, which is supported by our morphological studies. Figure 9(b) presents the modified Cole–Cole plots for the the PLAs, CPLAs and nanocomposites. The results showed that the slopes of the modified Cole–Cole plots of the nanocomposites prepared at higher screw speed (with higher extent of chain extension reaction) were smaller than those of corresponding samples prepared at lower screw speed (with higher acid value).

Elongational Behavior of the Blends and Nanocomposites

Elongational viscosity data for PLAs, CPLAs, blends and nanocomposites are shown in Figure 10. There is no sign of strain-hardening behavior for the PLA50 and PLA150 due to the linear chain structure of PLA. Higher elongational viscosity and weak strain-hardening behavior were observed for CPLA150 as compared to pure PLA. On the other hand, CPLA50 showed the lowest magnitude of elongational viscosity and its curve becomes more noisy due to the thermal degradation of PLA during reactive extrusion [Figure 10(a)]. Well-defined strain-hardening behavior was observed for the blends and nanocomposites [Figure 10(b,c)], with lower elongational viscosity values for blends as compared to their corresponding nanocomposites [Figure 10(d)].

The blends follow the same trend as chain extended PLA, regarding the effect of screw speed on the reaction. The elongational viscosities of CNPLA90 are slightly higher than those of CPLA90, probably because about 15 wt % of PLA in the nanocomposites passed through the extruder twice (due to masterbatch preparation). The elongational viscosity increased for nanocomposites upon increasing PBSA content, but it decreased for the blends. Also, increasing the screw speed caused the shear and elongational viscosities to increase for nanocomposites, but it caused a reduction for the corresponding blends, which is in agreement with acid value analyses. The maximum elongational viscosity was obtained for CNPLA70150 [Figure 10(c)], which showed the highest backbone peak base width [Figure 6(b)].

Mechanical Properties

Tensile tests were carried out to obtain the stress–strain curves. The results showed yield points for pure PLAs and CPLAs followed by instant rupture at low strain. The chain extender caused a small increase in the tensile strength of neat PLA. All the nanocomposites showed brittle fracture which could be attributed to the stress concentration due to the presence of intercalated tactoids at the phase interface, as discussed in the clay localization section (Figure 4). It should be interesting to consider lower clay concentrations and/or other nanoparticles to overcome this problem. On the other hand, all of the blends showed stable necking and ductile behavior. The strain at break values for the blends were noticeably higher than those of PLA, CPLA and corresponding nanocomposites (Figure 11). Moreover, the measured strain at break values for the blends prepared at higher screw speed were slightly higher than those of blends prepared at low screw speed. Tensile modulus values for nanocomposites, especially at low PBSA content, were higher than those for corresponding blends

CONCLUSION

Elongational flow and linear viscoelastic melt properties of the prepared samples were investigated and correlated with the composition, morphology and the extent of chain extension reaction. Improvements in the rheological and mechanical behavior were observed for PLA/PBSA blends with chain extender in reactive extrusion, as compared with neat PLA and chain extended PLA. Incorporation of nanoclay in the reactive blends raised the viscosities compared to the corresponding blends, with a larger effect for systems with higher PBSA content. The effects of screw speed on the chain extension reaction and consequently rheological and mechanical properties were investigated. The results suggest that lower screw speed favors the chain extension reaction for the blends, whereas higher screw speed is desirable for nanocomposite preparation. The importance of nanoclay presence is not only due to its effect on mechanical properties but, in the present case, it is also related to its barrier role to control the local concentration of chain extender in the PLA phase. Effective improvements in melt strength of PLA/PBSA blends, which makes it suitable for many polymer processing operations (e.g., film blowing, blow molding and fiber spinning), was achieved for the chain extended PLA/PBSA (70:30) nanocomposites prepared at high screw speed.

REFERENCES

1. Ge, H.; Yang, F.; Hao, Y.; Wu, G.; Zhang, H.; Dong, L. *J. Appl. Polym. Sci.* **2013**, *127*, 2832.
2. Hamad, K.; Kaseem, M.; Deri, F. *J. Polym. Res.* **2011**, *18*, 1799.
3. Ji, D.; Liu, Z.; Lan, X.; Wu, F.; Xie, B.; Yang, M. *J. Appl. Polym. Sci.* **2014**, *131*, 39580/1.
4. Lee, H. S.; Kim, J. D. *Polym. Compos.* **2012**, *33*, 1154.
5. Lee, J. B.; Lee, Y. K.; Choi, G. D.; Na, S. W.; Park, T. S.; Kim, W. N. *Polym. Degrad. Stab.* **2011**, *96*, 553.
6. Corre, Y.-M.; Duchet, J.; Reignier, J.; Maazouz, A. *Rheol. Acta* **2011**, *50*, 613.
7. Pivsa-Art, W.; Pavasupree, S.; O-Charoen, N.; Insuan, U.; Jailak, P.; Pivsa-Art, S. *Energy Proc.* **2011**, *9*, 581.
8. Al-Itry, R.; Lamnawar, K.; Maazouz, A. *Polym. Degrad. Stab.* **2012**, *97*, 1898.
9. Eslami, H.; Kamal, M. R. *Annu. Tech. Conf. Soc. Plast. Eng.* **2012**, *70th*, 155.
10. Eslami, H.; Kamal, M. R. *J. Appl. Polym. Sci.* **2013**, *129*, 2418.
11. Ojijo, V.; Sinha-Ray, S.; Sadiku, R. *ACS Appl. Mater. Interfaces* **2013**, *5*, 4266.
12. Eslami, H.; Kamal, M. R. *J. Appl. Polym. Sci.* **2013**, *127*, 2290.
13. Treece, M. A.; Zhang, W.; Moffitt, R. D.; Oberhauser, J. P. *Polym. Eng. Sci.* **2007**, *47*, 898.
14. Kamal, M. R.; Calderon, J. U.; Lennox, B. R. *J. Adhes. Sci. Technol.* **2009**, *23*, 663.
15. Demarquette, N. R.; Kamal, M. R. *Polym. Eng. Sci.* **1994** *34*, 1823.
16. Liu, C.; Jia, Y.; He, A. *Int. J. Polym. Sci.* **2013**, *2013*, 6.
17. Meng, Q.; Heuzey, M.-C.; Carreau, P. *J. Polym. Degrad. Stab.* **2012**, *97*, 2010.
18. Favis, B. D.; Chalifoux, J. P. *Polym. Eng. Sci.* **1987**, *27*, 1591.
19. Pötschke, P.; Paul, D. R. *J. Macromol. Sci. Part C* **2003**, *43*, 87.
20. Wu, D.; Lin, D.; Zhang, J.; Zhou, W.; Zhang, M.; Zhang, Y.; Wang, D.; Lin, B. *Macromol. Chem. Phys.* **2011**, *212*, 613.
21. Sumita, M.; Sakata, K.; Asai, S.; Miyasaka, K.; Nakagawa, H. *Polym. Bull.* **1991**, *25*, 265.
22. Katada, A.; Buys, Y.; Tominaga, Y.; Asai, S.; Sumita, M. *Colloid Polym. Sci.* **2005**, *284*, 134.
23. Van Oss, C. J.; Chaudhury, M. K.; Good, R. *J. Chem. Rev.* **1988**, *88*, 927.
24. Van Oss, C. J.; Good, R. J.; Chaudhury, M. K. *J. Colloid Interface Sci.* **1986**, *111*, 378.
25. Park, S.-J.; Seo, D.-I.; Lee, J.-R. *J. Colloid Interface Sci.* **2002**, *251*, 160.
26. Wu, D.; Yuan, L.; Laredo, E.; Zhang, M.; Zhou, W. *Ind. Eng. Chem. Res.* **2012**, *51*, 2290.
27. Khoshkava, V.; Kamal, M. R. *Biomacromolecules* **2013**, *14*, 3155.
28. Van Hooghten, R.; Gyssels, S.; Estravis, S.; Rodriguez-Perez, M. A.; Moldenaers, P. *Eur. Polym. J.* **2014**, *60*, 135.
29. Dharaiya, D.; Jana, S. C. *Polymer* **2005**, *46*, 10139.
30. Park, S. J.; Seo, D. I.; Lee, J. R. *J. Colloid Interface Sci.* **2002**, *251*, 160.
31. Gui, Z.-Y.; Wang, H.-R.; Gao, Y.; Lu, C.; Cheng, S.-J. *Iran. Polym. J.* **2012**, *21*, 81.
32. Dae Han, C.; Kim, J. K. *Polymer* **1993**, *34*, 2533.